analytical chemistry

Article

pubs.acs.org/ac

Optical pH Sensor Covering the Range from pH 0–14 Compatible with Mobile-Device Readout and Based on a Set of Rationally Designed Indicator Dyes

Raúl Gotor,[†] Pichandi Ashokkumar,[†,‡] Mandy Hecht,[§] Karin Keil, and Knut Rurack*

Chemical and Optical Sensing Division, Bundesanstalt für Materialforschung und -prüfung (BAM), Richard-Willstätter-Strasse 11, 12489 Berlin, Germany

Supporting Information

ABSTRACT: In this work, a family of pH-responsive fluorescent probes has been designed in a rational manner with the aid of quantum chemistry tools, covering the entire pH range from 0–14. Relying on the boron–dipyrromethene (BODIPY) core, all the probes as well as selected reference dyes display very similar spectroscopic properties with ON–OFF fluorescence switching responses, facilitating optical readout in simple devices used for detection and analysis. Embedding of the probes and reference dyes into hydrogel spots on a plastic strip yielded a test strip that reversibly indicates pH with a considerably small uncertainty of ~0.1 pH units. These strips are not only reusable but, combined with a 3D-printed case that can be attached to a smartphone, the USB port of which drives the integrated LED used for excitation, allows for autonomous operation in on-site or in-the-field applications; the developed Android application software ("app") further simplifies operation for unskilled users.

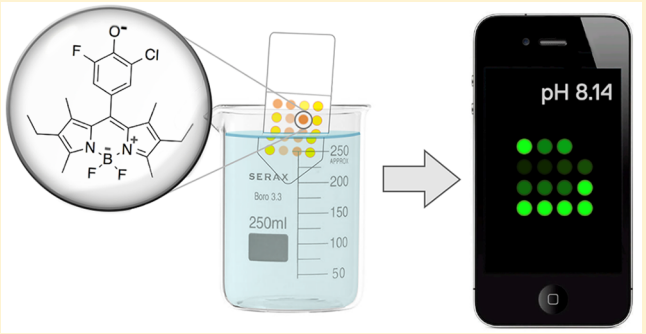

The pH value is among the few chemical parameters that are ubiquitously of high importance. Whether the availability or mobility of inorganic ions for organisms or in environmental compartments is concerned,[1−3] processes in wastewater management, the biotechnological or chemical industry,[4−6] physiological processes in organisms, both vital and detrimental or between organisms and their environment,[7−10] global ecological or intracellular regulatory scenarios,[11−13] pH is often decisive.

Among the different systems for pH measurement, the pH glass electrode is by far the one most commonly used.[14] Nonetheless, glass electrodes often show a rather poor performance in both extremes of the pH scale, especially in the highly alkaline region and have to be recalibrated in a discontinuous way.[15] Optical pH sensors or optodes can be a good alternative here. Such sensors operate through changes in their optical properties such as absorption, fluorescence, or reflectivity upon variations in pH.[16,17] In recent years, fluorescence sensors have become predominant because they are simple to implement and offer high sensitivity and specificity. Basically, an embedded fluorophore undergoes either a spectral or intensity change upon reversible protonation/deprotonation.

The optical response of a fluorescent pH indicator is a function of the concentration of the acidic and basic forms of the indicator,[18] which follows the Henderson–Hasselbalch equation. This results in a sigmoidal response function with a dynamic working range of commonly 2 pH units, which only allows for the determination of pH values in specific pH windows.[19] Researchers have thus conceived various strategies to broaden the pH range of optical indicators by the use of polyprotic dyes or metal–organic frameworks,[20,21] the multilayer adsorption of indicators,[22] pH-triggered aggregation-induced emission,[23] conjugated or block copolymers bearing sensing units,[24,25] the use of artificial neural networks,[26] the modulation of the curvature of hollow mesoporous silica particles with affixed sensing units,[27] quantum or carbon dots,[28,29] or mixtures of spectroscopically compatible indicators for different pH ranges.[30−35] The latter is not only also the longest known concept since the establishment of broadband pH papers in the 1920s[36] but has been realized in a multitude of ways by combining various dyes of different classes with suitably differing pK_a in a single membrane[36] or in individual elements of a membrane[33] as well as by using derivatives of a single dye class with selected pK_a, embedded in molecular[30,32] or particle-bound[30,34,35] form in thin sensor films (for a more detailed overview, see Section S1, Supporting Information).

However, among the large amount of optical pH sensors reported, only very few cover a range of ≥10 pH units and all of these systems rely on the combination of dyes with different pK_a values.[26,30,32−34] To achieve a linear response over the desired pH range, ΔpK_a between consecutive indicators should

Received: May 19, 2017
Accepted: July 11, 2017
Published: July 11, 2017

DOI: 10.1021/acs.analchem.7b01903
Anal. Chem. 2017, 89, 8437–8444

not exceed 1.7.[37] The latter directly points to the major constraint in this regard, i.e., the still existing lack in photochemically stable fluorescent dyes with pK_a in the highly alkaline region at pH > 10;[38−40] for examples in absorbance, see refs 41 and 42.

On the basis of our recent activities in the field,[39,43] we became interested in devising a flexible broadband pH sensing system that can potentially be implemented in various simple devices, the simplest perhaps being strips,[44] and that can yield quantitative information in a reliable manner with the help of only a simple aid such as widely available mobile communication devices used in everyday life. Since a suitable dye unit shall be at the heart of such a system, we opted for boron−dipyrromethene or BODIPY dyes, which possess advantageous properties, such as high thermal and photostability, high brightness in a suitable optical window, facile synthetic modifiability, and possess favorable octanol−water partition coefficients for final steric immobilization in a polymeric sensing matrix.[45−47]

Here, we present a series of such BODIPY pH indicators (Chart 1), most of them newly designed in a rational fashion, and their integration into a strip-based array via hydrogel embedding that allows for reversible quantitative pH measurement over the entire range from pH 0 to 14 utilizing a conventional smartphone.

Chart 1. Chemical Structures of the Dyes in This Work; Nomenclature: 1−10 Are the Probes Used in the Final Assays, R1−R3 Are the Reference Dyes Used Accordingly, In1−In7 Are Indicator Dyes Not Finally Used in the Assay on Strip

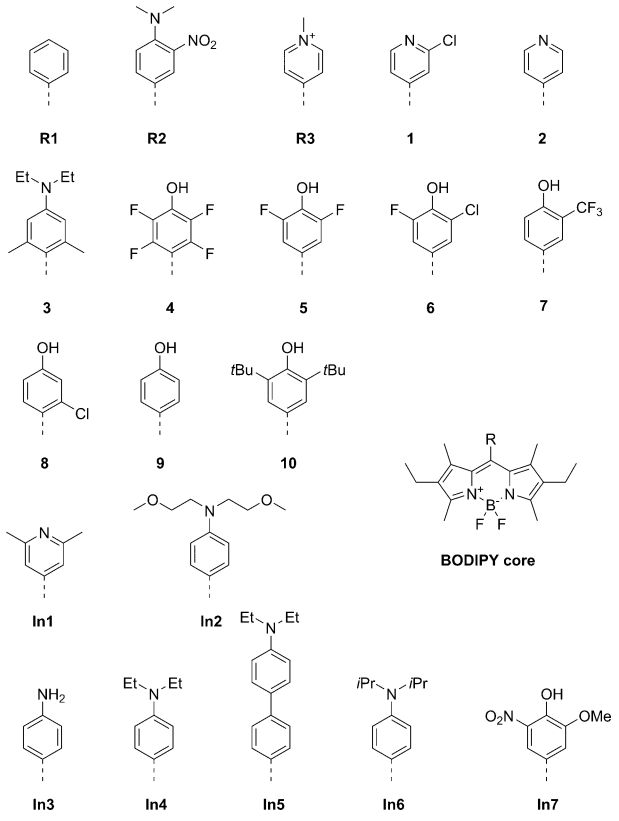

EXPERIMENTAL SECTION

Materials, Methods, and Instrumentation. Reagents for synthetic procedures were obtained from commercial suppliers and used without further purification, unless indicated otherwise. Air- and moisture-sensitive reactions were carried out with previously dried materials under N_2 atmosphere. When required, solvents were dried for 24 h over 3 Å molecular sieves. All details on syntheses and compound characterization are collected in Sections S1 and S9, Supporting Information.

UV−vis absorption spectra were recorded on a Specord 210-Plus spectrophotometer from Analytik Jena. Steady-state fluorescence measurements were carried out on a FluoroMax-4 spectrofluorometer from Horiba Jobin-Yvon, using standard 10 mm path length quartz or PMMA cells. All the solvents employed for the spectroscopic measurements were of UV spectroscopic grade (Aldrich). Schott Nexterion Slide E and PolyAn 3D-Epoxy Slides were used as solid supports for the dye-doped hydrogel and were cut into 10 mm strips which fit into commercially available PMMA cells. The hydrogel HydroMed D4 (ether-based hydrophilic urethane, water content 50%) was received from AdvanSource Biomaterials Corp.

Preparation of Dye-Coated Strips. In total, 0.5 g of HydroMed D4 were dissolved in a mixture of 5.4 g of EtOH and 0.6 g of H_2O by mechanical mixing for 24 h to ensure homogeneity. Then, 398 μL of 1,4-dioxane stock solutions of the dyes (**1−10**, **R1−R3**, **In1−In7**; c = 2.5 mM) were added to the hydrogel solution to achieve dye concentrations of 2 μmol g^{-1} of polymer. The mixture was stirred additionally for 1 h before dip-coating the epoxy functionalized polymer slides. Excess hydrogel was removed by placing the strips vertically over absorbing paper before air-drying the strips for 3 h prior to use.

Preparation of Array Containing Dye Membranes. Viscous hydrogel solutions were prepared by dissolving 4.0 g of HydroMed D4 in a mixture of 21.6. g of EtOH and 2.4 g of H_2O by mechanical mixing for 24 h. Then, 4 μL of 1,4-dioxane stock solutions of each dye (**1−10**, **R1−R3**, **In1−In7**; c = 32.2 mM) were added to 1 mL vials containing the viscous hydrogel. After 1 h of agitation, 12.5 μL of each solution was carefully placed in a corresponding well on a custom-made poly(methyl methacrylate) (PMMA) strip and allowed to dry for 3 h. The deposited amount of dye-containing hydrogel was experimentally optimized to ensure a flat membrane surface after drying, thus avoiding inhomogeneities due to meniscus formation.

pK_a Determination in Solution and in Membranes. Neat solutions (≤10 μL) of dyes **1−10** and **In1−In7** in 1,4-dioxane (32.2 μM) were added into quartz cells containing an H_2O−EtOH 1:1 (v/v) mixture while keeping the resulting amount of 1,4-dioxane below 0.4% and the optical density of the solution at $\lambda_{abs}^{max} \leq 0.1$ ($c_{dye} \sim 1$ μM). Aliquots of 0.01−1 M KOH (for 4-hydroxyphenyl-based dyes **5−10**) or 0.01−1 M HCl (for dyes **1−4** and **In1−In7**) in the solvent mixture were added to the solutions under mechanical stirring, while the pH was constantly monitored with a digital pH meter (pH lab 827, Metrohm) equipped with a glass electrode (Biotrode). Absorption and fluorescence spectra were taken after addition of each aliquot. For the final analysis, pH values in the solvent mixture were activity-corrected as detailed in ref 39. For the pK_a measurements of the dye-doped hydrogels, the coated polymer slides containing the different dyes were introduced into PMMA cells in a 45° geometry. The cells were filled with 2.5

DOI: 10.1021/acs.analchem.7b01903
Anal. Chem. 2017, 89, 8437−8444

Table 1. Spectroscopic Properties and pH-Responsive Behavior of the Dyes Presented in This Work[a]

probe	λ_{abs}[nm] sol.	λ_{em} sol.	[nm] λ_{abs} [nm] D4	λ_{em}[nm] D4	Φ_f^{ON} sol.	Φ_f^{OFF} sol.	pK_a[b] sol.	pK_a[c] D4	FEF sol.	FEF D4
R1	524	537	527	540	1.00	–[d]	–[d]	–[d]	–[d]	–[d]
R3	537	645	538	633	0.03	–[d]	–[d]	–[d]	–[d]	–[d]
R2	532	539	534	548	<0.01	–[d]	–[d]	–[d]	–[d]	–[d]
1	531	550	530	548	0.55	0.01	0.95	0.50	22	1.8
2	529	545	531	545	0.64	0.15	2.15	2.30	99	35
In1	528	546	530	543	0.88	0.17	3.33	2.34	49	16
In2	528	541	528	541	0.86	<0.01	1.55	0.95	174	1.4
In3	527	539	529	540	0.76	<0.01	2.87	2.11	58	2.4
In4	528	544	530	542	0.85	<0.01	4.46	2.82	233	2.6
In5	525	539	529	539	0.75	0.03	4.62	2.98	36	2.5
3	529	540	527	540	0.98	<0.01	4.62	3.29	317	7.2
In6	528	541	530	541	0.90	0.08	5.75	4.67	7	1.8
4	540	553	543	554	0.96	<0.01	5.13	6.11	193	5.4
In7	529	542	532	541	<0.01	<0.01	6.09	7.05	10	6.4
5	528	540	531	541	0.85	<0.01	7.40	8.43	923	31.9
6	528	541	534	541	0.98	<0.01	7.13	8.91	630	18.7
7	526	538	530	540	0.89	<0.01	8.75	9.96	138	21.0
8	530	541	533	541	0.96	<0.01	9.33	10.58	207	98
9	523	532	526	534	0.90	<0.01	9.98	11.44	332	205
10	522	533	525	535	0.93	<0.01	13.10	12.83	51	20

[a]Only the optical properties of the dyes in its ON state are shown. (sol.) stands for solution (H_2O–EtOH 1:1 v/v), (D4) stands for polyurethane hydrogel, FEF stands for fluorescence enhancement factor; for fluorescence lifetimes of selected ON states, see Table S7; **R1** in CH_2Cl_2 (Φ_f = 0.95) was used as reference for the quantum yield calculations.[57] [b]Uncertainty of measurement ± ≤0.04. [c]Uncertainty of measurement ± ≤0.05. [d]Not applicable.

mL of MiliQ water, and the pH was modulated following the above procedure with an additional manual stirring, followed by absorption and emission measurements after each pH step.

pH Measurements with Smartphone. pH measurements with smartphone read-out were performed with a self-written Android program installed in a Samsung Galaxy S II (GT-I9100). The program (or app) calculates the pH according to a previously taken picture of the strip. After photographing, the app recognizes the different pH indicators, evaluates the emission intensity of each individual probe, and computes the pH by processing these values in the Henderson–Hasselbalch equation.

Prior to the start of the measurements, the strips were soaked in water for 120 s and then immersed in the test solution for 150 s. After removal of the strip from the solution, any excess water was removed with absorbing paper. An image was then recorded using only the zoom function, when necessary, after placement of the strip in the holder attached to the smartphone. The entire pH range was measured by employing aqueous solutions buffered at pH values of 0.51, 1.23, 2.02, 2.51, 3.02, 3.54, 4.07, 4.58, 5.08, 5.58, 6.08, 6.49, 7.01, 7.52, 7.98, 8.49, 9.03, 9.57, 9.89, 10.20, 10.87, 11.76, 12.42, 12.95, 13.37 (±0.03). After the experiments, the strip was stored in a closed box, avoiding unnecessary exposure to light. When stored in day light, photobleaching has not been observed for up to 2 weeks.

Computational Details. Optimization of the S_0 ground-state geometries in the gas phase was performed with the density functional theory (DFT) method employing the hybrid functional B3LYP with a 6-31G basis set and energy minimized as implemented in Gaussian 03.[48]

pK_a Correlation and Prediction. As suggested by Seybold and co-workers,[49] Mulliken charges of the OH group in the phenol series (Q_{OH}) and the amino substituent in the aniline series (Q_{An}; for detailed description, see Section S3, Supporting Information) were used for the correlation with the experimentally determined pK_a values. A pyridine series was not explicitly modeled, because these three dyes were finally only chosen to fill the gap in the highly acidic region, on the basis of recent findings by Bartelmess et al.[50]

RESULTS AND DISCUSSION

Since the early works by Wolfbeis' group and us,[38,51] many proton-responsive BODIPY dyes have been described, most of them acting through appended phenol, aniline, or pyridine groups.[50,52−54] While systematic tuning of the pK_a of such dye families has frequently been realized, the $\Delta^{max}pK_a$, defined as difference between the two dyes with the highest and lowest pK_a, achieved for such series commonly amounted to ≤2, irrespective of the pH-active unit.[50−52] Only the recent broadband approach of Klimant's group that relies on aza-BODIPYs shows a more promising $\Delta^{max}pK_a$ ∼ 5 in H_2O–EtOH 1:1 solution ($\Delta^{max}pK_a$ ∼ 4 in hydrogel) for the integrated phenol moieties.[32] Since the use of different dye classes in broadband sensors often entails problems already because of different solubilities in the matrix material, pH-responsive subunit tailoring seemed the best option to us. However, attempting a maximum $\Delta^{max}pK_a$ > 5 in such a series, we did not embark on extensive syntheses. Instead, we invoked a rational approach by first synthesizing only two derivatives of a single family and correlating the measured pK_a to a suitable parameter derived from quantum chemical calculations of the respective dyes. Then iterative modeling of other derivatives, prediction of their pK_a and synthesis of the most promising target dyes were carried out to yield a library of 17 dyes synthesized in total, constituting a matrix of indicators that covers the whole pH range with pK_a between 0.5 and 12.8 (in the final hydrogel formulation). In contrast to Klimant's group,

DOI: 10.1021/acs.analchem.7b01903
Anal. Chem. 2017, 89, 8437–8444

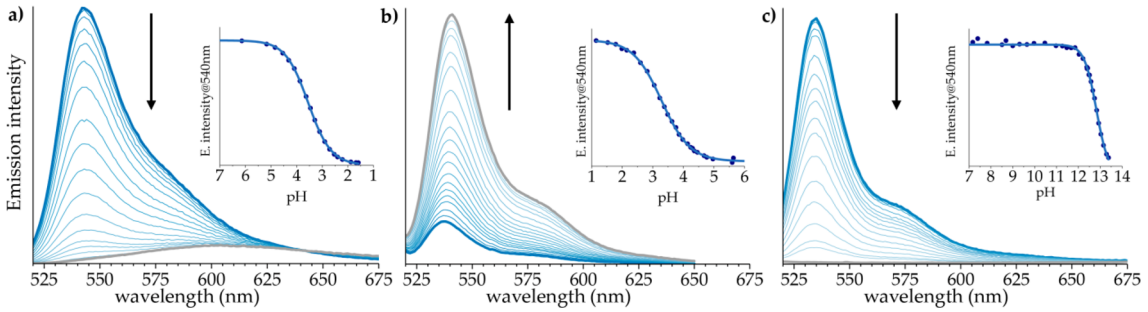

Figure 1. Fluorescence spectra (λ_{exc} = 500 nm) and titration profiles of a sensor film containing (a) **In1**, (b) **3**, and (c) **10** immersed in water at different pH. The pH of the solutions was modulated from neutral to ~pH 1 by subsequently adding small aliquots of HCl solution (0.01−1.00 M, parts a and b) or from neutral to ~pH 14 by subsequently adding small aliquots of KOH solution (0.01−1.00 M, part c). The thick blue line corresponds in all cases to the spectrum of the dye in its neutral form, while the thick gray line represents the spectrum of the dye as ionic species. The insets show the fluorescence intensity at λ_{em} = 540 nm plotted as a function of pH.

we chose the 1,2,3,5,6,7-hexaalkylated BODIPY core as the basic chromophore and coupled the pH-responsive unit through the 8- (also called meso-) position (Chart 1). Such dyes are not only straightforward to synthesize and absorb and emit well in the visible range of the spectrum with very high brightness but can also be very easily tuned toward the red by 3,5-substitution or toward higher hydrophilicity by difluoride exchange,[43,55] rendering them very versatile for future adaption to other applications. In essence, all BODIPYs were prepared by common synthetic procedures[45] using the corresponding aldehyde derivatives (see Section S8, Supporting Information).

Chart 1 collects the prepared compounds: **4**−**10** and **In7** belong to the phenol series, **3**, **In2**−**In6**, and **R2** to the aniline series, **1**, **2**, and **In1** to the pyridine series, **R3** is a permanently cationic pyridinium dye, and **R1** the nonresponsive meso-phenyl parent dye.

Spectroscopic Properties and Photophysics. All the dyes in this study share the characteristics of the 1,3,5,7-tetramethyl-2,6-diethyl-BODIPY core, i.e., strong lowest-energy absorption and intense emission bands at ~530 ± 10 and 540 ± 10 nm, respectively. The advantage of sharing the same core endows the whole system with simplicity as only single excitation and emission wavelengths are required for interrogation of all the dyes. We chose the hexaalkylated core because it is the brightest and most photostable one among the core-alkylated BODIPYs. Especially the methyl groups attached to the 1,7-positions guarantee a minimal influence of the responsive group in the meso-position on the spectral features of the dyes, because it is perpendicularly oriented, i.e., electronically virtually decoupled.[51] Although possessing very diverse electronic features, the meso-substituents act thus only through minor inductive effects on the spectral band positions of the 17 dyes.

Water−EtOH solutions (1:1 v/v, c_{dye} = 1 μM) of all the dyes showed intense and narrow absorption spectra, indicating that the dyes are neatly dissolved in this medium and that aggregation does not occur. In accordance with BODIPY photophysics, the main absorption band was assigned to the intense $S_1 \leftarrow S_0(\pi\pi^*)$ transition, together with the accompanying vibronic shoulder at ~1200 cm^{-1} higher energies (Figure S7). Emission occurs from a BODIPY-localized excited state (LE) at ~540 nm. Strongly red-shifted emission bands that are known to arise for meso-aniline-substituted BODIPYs especially in aprotic organic solvents because of an intramolecular charge transfer (ICT) process in the excited state have not been observed during our studies in either mixed aqueous or hydrogel matrixes. The Stokes shifts of 7−13 nm are small for all the dyes, stressing the high rigidity of the core and the structural resemblance of the ground and excited states. Nonradiative deactivation pathways are thus negligible, which is reflected by the high fluorescence quantum yields in the ON state (Table 1; see below for a more detailed discussion).

pH-Responsive Behavior. For the phenol- and pyridine-containing dyes, the neutral state is the highly fluorescent ON state. Ionization of these dyes, either by deprotonation to yield the phenolate (**4**−**10**, **In7**) or by protonation of the pyridine-N (**1**, **2**, **In1**), then produces a strong quenching. Figure 1 and Figure S6 reveal that in case of the phenol−phenolate transition, the shape of the absorption band remained unchanged and only the spectrum was displaced by ~5 nm to shorter wavelengths. The emission band was virtually unchanged, the intensity gradually decreasing with increasing degree of deprotonation. As can be deduced from Table 1, the OFF states of the phenol series are virtually nonfluorescent (Φ_f < 0.01), resulting in a very efficient ON−OFF switching with factors up to several hundred (Figure 1c). Mechanistically, these features can be explained with deprotonation shifting the molecular orbitals (MO) localized only on the meso-substituent energetically upward so that they become HOMO and HOMO−1 (Figures S9 and S10). Accordingly, if a BODIPY-centered excitation from HOMO−2 or lower into LUMO occurs, photoinduced electron transfer (PET) from the meso-group can efficiently quench the fluorescence without noticeable spectral changes as is well-known for such virtually decoupled PET probes.[56] A detailed discussion is given in Section S8, Supporting Information.

For the pyridine series, the situation is comparable yet reversed. Protonation leads to meso-group localized MOs being shifted downward, in between the BODIPY-localized MOs. Whereas HOMO−2, HOMO−1, HOMO and LUMO are BODIPY-localized in **2** and only HOMO−3, LUMO+1, and LUMO+2 are pyridine-localized, all MOs from HOMO−7 to HOMO yet next only LUMO+2 are BODIPY-localized in $\mathbf{2H^+}$; now, LUMO and LUMO+1 are pyridine-localized. The latter thus act as efficient acceptors for an electron having been excited into the BODIPY-centered LUMO+2 (Figures S9 and S10). Since the direct HOMO−LUMO transition is strongly forbidden due to the perpendicular arrangement of both molecular fragments, the red-shifted and very weak fluorescence of the protonated OFF state presumably arises from an excited-state ICT process as has been proposed by Harriman et al. (Figure 1a).[58] The decrease upon protonation is

DOI: 10.1021/acs.analchem.7b01903
Anal. Chem. 2017, 89, 8437−8444

accompanied by a strong bathochromic shift in emission (82 and 55 nm for **2** and 62 and 34 nm for **In1** in solution and hydrogel, respectively), while absorption shifts were negligible with 5 and 7 nm for **2** and **In2**. The latter observation supports the mechanistic assumption of an ICT process being active in the excited state, possibly connected to a less twisted conformation. Because of the formation of the new ICT emission band, these compounds are not completely dark in the OFF state. In contrast, no distinct spectral shifts in absorption or emission were noticed for **1**, only protonation-induced quenching, with the exact mechanism being yet still unclear.

Opposite to the pyridine derivatives, the aniline dyes suffer from fluorescence quenching through a PET-like mechanism in their neutral form, i.e., they are in the OFF state when deprotonated, showing virtually no emission (Figure 1c).[51,56] If the molecules are protonated at the aniline moiety, the PET process is blocked and the fluorescence restored, switching the OFF state back ON. The data in Table 1 suggest that the OFF state of some aniline dyes is not as efficiently quenched as that of the phenol dyes. The latter is attributed to hydrogen bonding interactions of water and/or ethanol molecules solvating the dye with the lone electron pair of the aniline-N, in line with previous observations.[59] All the dyes were subjected to pH titrations, and the resulting pK_a data together with the fluorescence enhancement factors (FEF) are collected in Table 1. As can be seen, the probes covered pK_a from 0.95 to 13.1 with the FEF reaching a maximum value of >900.

Hydrogel. As mentioned above, the chemical nature of the hexaalkylated BODIPY core is ideally suited for steric embedding into polar matrixes while avoiding leaching in aqueous solutions. Urethane hydrogels are such a matrix and thus the probes and dyes were embedded at 2 μmol g^{-1} of polymer. The spectroscopic properties of the dyes remained virtually identical, i.e., the absorption and emission maxima were only slightly shifted by ≤4 nm to the red for the acidic dyes **4**−**10** or to the blue for the basic dyes **1**−**3**, **In1**, **In2**, and **In4**−**In6** while no broadening was observed. These findings were attributed to the slightly lower polarity of the hydrogel compared to H_2O−EtOH mixtures. The pK_a data of all the dyes embedded in the hydrogel matrix are also presented in Table 1. The data reveal that the pK_a of the aniline- and pyridine-based probes are lower in the hydrogel matrix when compared to neat solution, whereas an opposite trend is observed for the phenol based probes, most likely arising from the different microenvironment and altered proton mobility.

Smartphone-Based pH Sensing. At present, the scientific community is beginning to take more and more advantage of smartphone-based sensing and chemometrics. This is basically rooted in the fact that these devices are equipped with rather powerful cameras and have their own data acquisition, analysis, and transmitting units on board. Not only is the device rather low-cost and already in the hand of a large number of potential users but its command does not require a specifically skilled user. Analytical applications for smartphone readouts are thus becoming increasingly popular,[60−62] among them also first attempts to measure pH.[63,64] However, as with every rapid test for everyday use, reliability and unequivocal quantification are essential requirements that the combination of chemical test and mobile devices finally have to master for the technology to become widely accepted in society. When using a smartphone CMOS for measuring fluorescence, the limitations in sensitivity and resolution have to be considered. Additionally, the CMOS module driver autocompensates for different light inputs with a variation of the integration times (exposure times), making the reproducible obtaining of unreferenced values challenging. Therefore, the "ideal" fluorescent probe for a smartphone application should fulfill certain requirements: high fluorescence quantum yield, strong switching between ON and OFF states of the probe, and a low to negligibly intensity in the OFF state. Finally, if this probe is to be combined with others in an actual multiprobe sensor matrix, the probes should at best show rather similar spectroscopic features to better fit into the same exposure window.

Among the dyes developed in this work, **1**−**10** meet these requirements. For all of them, $\Phi_f^{ON} \geq 0.55$ (in solution) and $5 < \Delta\Phi_f^{ON-OFF} < 210$ (in hydrogel).[65] Moreover, the absorption and fluorescence colors of the ON states are also rather uniform with $\lambda_{abs}^{max} = 531 \pm 5$ nm and $\lambda_{em}^{max} = 543 \pm 6$ nm for the 13 dyes **1**−**10** and **R1**−**R3** in the hydrogel (Figures S6 and S7). Accordingly, because probes **1**−**10** cover the entire pH range with intervals of <2.0 pH units between them (Figure S3), we proceeded with their integration into a broadband pH strip for smartphone analysis. Because of the lack of probes ideally matching pK_a 4 and 7, we mixed the two neighboring probes to get those required pK_a values (Figure 2 and Figure S3).

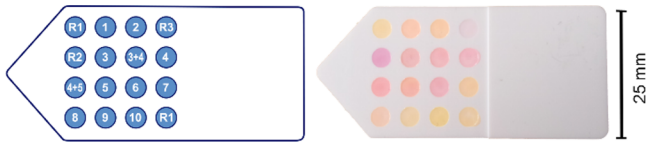

Figure 2. Final configuration of the sensor and reference spots containing **1**−**10** and **R1**−**R3** on the PMMA strip. The 16 wells were arranged in a 4 × 4 fashion, with a grid size of 8 mm. The dimensions of the wells were height = 50 μm, diameter = 5 mm.

Additionally, the matrix implemented on the custom-made strip includes dyes **R1**, **R2**, and **R3** as internal references, i.e., as ON reference for dyes **1**−**10**, general OFF reference and specific OFF reference for **1** and **2**, respectively. For the preparation of the sensor strip, the probes and reference dyes were dissolved in a more viscous hydrogel, and 12.5 μL of these viscous gels were placed in the sensing spots on a homemade PMMA strip in the configuration shown in Figure 2.

Software. A smartphone application ("app") was programmed in Java programming language, on Android Studio 2.0 using Android SDK tools API 22 (Android 5.1),[66] to facilitate matrix readout and data analysis. Operation of the app is straightforward and user-friendly. After starting the app, the field of view of the smartphone camera is displayed on the screen. The user is requested to insert the strip into the measurement chamber and to start the measurement with the "shoot" button. After the image analysis, the pH of the strip is displayed on the screen (Figure S1).

Image Analysis. Measurement of the different sensing spots is done by analyzing the luminance ($\overline{Y}$) values of dyes **3**−**10**, while in the case of the pyridine-based dyes **1** and **2**, which produce a strong shift in the fluorescence emission wavelength, the hue parameter (H) is measured. The representative values of the samples (v_s^r), either luminance or hue, are then mapped against the representative values of the corresponding ON (v_{ON}^r) and OFF (v_{OFF}^r) references, yielding a quantitative value proportional to the fraction of probes in the ON state.

Calibration. As mentioned before, actual smartphone camera modules are equipped with a hard-coded autoexposure compensation to achieve a better color distribution based on

DOI: 10.1021/acs.analchem.7b01903
Anal. Chem. 2017, 89, 8437−8444

the observed histogram. In extreme situations in which all probes in the matrix are at either ON or OFF, the observed light at the CMOS is very extreme in the sense that the autoexposure compensation system is triggered. A measurement of these extreme values can only be performed if a correction step is applied subsequently. The latter is based on the luminance relation between the probes and their ON and OFF references. These corrections factors are obtained from calibration measurements at pH 1 and pH 13. They only need to be registered once for every strip (see section S4.5, Supporting Information).

pH Determination with External $UV_{365\ nm}$ Lamp as Excitation Source. For a first performance assessment, solutions of different pH were measured with the strip using a laboratory UV cabinet at 365 nm with a power of 1 mW cm^{-2} as the light source. The smartphone was placed on top of the cabinet with the camera facing down so that the strip could be placed inside the cabinet and viewed through the glass window, introducing a distance of ~150 mm between strip and camera. Each experiment was repeated 3 times and the obtained values are plotted vs those measured with a pH electrode in Figure 3.

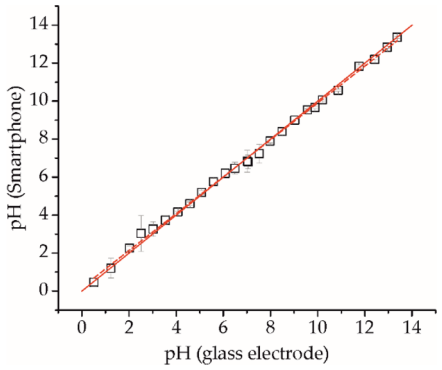

Figure 3. Comparison of pH values obtained with the smartphone photographing the sensor strip under illumination in a UV cabinet and a conventional pH glass electrode. Solid and dashed show the ideal and real fits, respectively. Values are the average of 3 independent runs.

The correlation of the data obtained by both methods is very good, yielding a linear fit with $r^2 = 0.997$ and a slope of 0.971. The average uncertainty was determined to 0.16 pH units. To address the strips' batch to batch reproducibility, the experiment was repeated with three other strips, yielding a standard deviation between strips of <0.20 pH units. A typical response pattern of the intensity changes of the matrix of spots is shown in Figure 4.

pH Determination with Customized Smartphone Case Integrating Excitation Source. A case mountable over the top end of the smartphone cover and containing a measurement chamber into which the strip could be inserted was designed and printed with a 3D printer. The chamber accommodates all optical elements and a slot for strip insertion. A case-mounted LED (470 nm) driven by 20 mA through the smartphone's micro-USB connector with a wire setup in the OTG mode serves as the excitation source, at a distance from the strip of approximately 60 mm. The light is guided through a small polyethylene diffuser and selected by a 492 nm short-pass filter (Semrock, 492 nm blocking edge, BrightLine, 1-in.) before it hits the sensor strip at an angle of 45°. The fluorescence is collected by the smartphone CMOS, placed at 0° and 47 mm over the strip, after having been selected by a

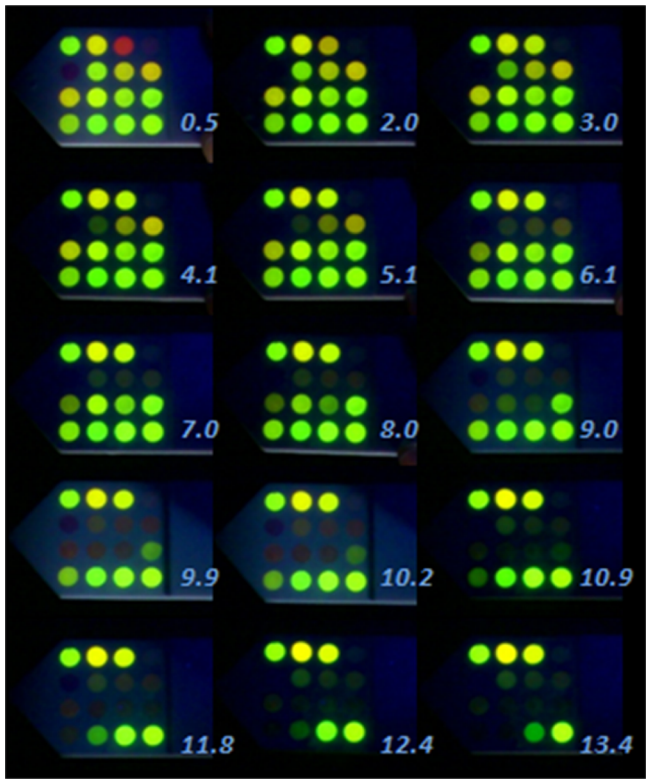

Figure 4. Combination of different images taken of a strip at different pH values as indicated. The strips were placed inside of the UV cabinet and irradiated at 365 nm. Slight color shifts can be noticed especially for the pyridine-based dye **2**.

550 nm band-pass filter (Semrock, 550/49 nm BrightLine, single-band bandpass, 1-in.); a detailed schematic is included in Section S5, Supporting Information, Figures S4 and S5.

The procedure for the pH measurement with the smartphone and the adapter was similar to the procedure described before for the UV cabinet/smartphone combination. First, the strips were calibrated at both extremes of the pH scale. Then, after dipping the strip into the desired aqueous solution, the excess of water was removed with absorbing paper (conventional Kleenex placed over the strip), and the strip was inserted into the slot. Three replicates were performed with three different strips. In Figure 5, the pH values measured with the smartphone are plotted against those measured with the glass electrode.

Reversibility. The system developed here implies that it can be used more than once, i.e., is different from disposable pH paper strips. We thus demonstrated that repetitive measurements are possible by exposing a strip 10 times to alternating pH values, cycling between pH 2.51 and pH 10.20. At those pH, most of the dyes are in their ionic form, which should increase their solubility in water compared with the neutral form, yet no tendency for leaching or washing out was observed. Apart from the uncertainties of measurement, the pH values were correctly reproduced (pH 2.58 ± 0.17 and pH 10.32 ± 0.22, Figure S8), showing that the sensor is reversible and stable across very broad pH changes.

■ CONCLUSIONS

A library of 17 (2,6-diethyl-1,3,5,7-tetramethyl)-BODIPY pH probes has been developed in this work, to cover the full scale for pH measurement in aqueous solution. The probes have

DOI: 10.1021/acs.analchem.7b01903
Anal. Chem. 2017, 89, 8437−8444

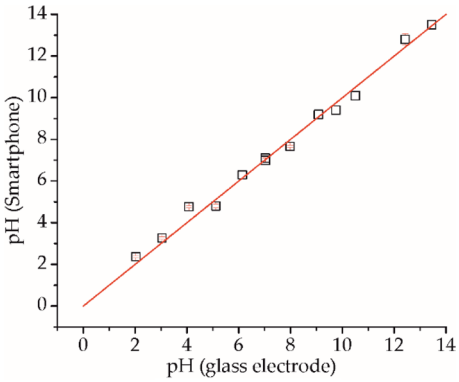

Figure 5. Comparison of pH values obtained using the smartphone with strip holder and a conventional pH glass electrode. Ideal and real fits coincide. Values are the average of 3 independent runs.

been chosen for matching excitation/emission wavelength ranges while at the same time possessing the typical robustness and outstanding optical properties of BODIPY dyes. The pH sensing capabilities have been demonstrated in solution and for individual polymeric slides coated with a hydrogel mixture containing selected probes. Taking a step toward general applicability, a group of these dyes has been embedded into the hydrogel sensor spots on the strip, the fluorescence response of which can be read by a smartphone application using different illumination sources. Thus, we have demonstrated the possibility of obtaining precise pH readouts after taking pictures of the strip with the smartphone, in particular by using a 3D-printed smartphone adapter incorporating all the required optical elements that can be driven by the phone itself, allowing for autonomous use on site. The present system responds in a reversible manner and can be reused multiple times while showing favorably low uncertainties. It is obvious that all integral parts of the system, the pH-responsive dyes, the smartphone measurement setup, and the concept of internal referencing with an automated data analysis and interpretation software tool can be used for many other purposes.[68] Current work in our laboratory is exploiting these features in various ways.

■ ASSOCIATED CONTENT

Supporting Information

The Supporting Information is available free of charge on the ACS Publications website at DOI: 10.1021/acs.analchem.7b01903.

Synthetic procedures, absorption, emission spectra and lifetimes of the dyes, pK_a predictions, photophysics, pH titrations, and strip and smartphone adapter design (PDF)

■ AUTHOR INFORMATION

Corresponding Author

*E-mail: knut.rurack@bam.de.

ORCID

Knut Rurack: 0000-0002-5589-5548

Present Addresses

‡P.A.: Laboratory of Biophotonics and Pharmacology, Faculty of Pharmacy, University of Strasbourg, UMR CNRS 7213, 74 Route Rhin, F-67401 Illkirch-Graffenstaden, France.

§M.H.: Surflay Nanotec GmbH, Max-Planck-Strasse 3, D-12489 Berlin, Germany.

Author Contributions

†R.G. and P.A. contributed equally.

Notes

The authors declare no competing financial interest.

■ ACKNOWLEDGMENTS

We gratefully acknowledge financial support by the Alexander-von-Humboldt Foundation (P.A.) and the Spanish MICINN (R.G.) as well as fruitful discussions with A. Costero (Universidad de Valencia).

■ REFERENCES

(1) Jackson, L. J. *Sci. Total Environ.* **1998**, *219*, 223−231.
(2) Peng, J.; Song, Y.; Yuan, P.; Cui, X.; Qiu, G. *J. Hazard. Mater.* **2009**, *161*, 633−640.
(3) Rivett, M. O.; Buss, S. R.; Morgan, P.; Smith, J. W. N.; Bemment, C. D. *Water Res.* **2008**, *42*, 4215−4232.
(4) Kurniawan, T. A.; Chan, G. Y. S.; Lo, W.-H.; Babel, S. *Chem. Eng. J.* **2006**, *118*, 83−98.
(5) Stergiou, P.-Y.; Foukis, A.; Filippou, M.; Koukouritaki, M.; Parapouli, M.; Theodorou, L. G.; Hatziloukas, E.; Afendra, A.; Pandey, A.; Papamichael, E. M. *Biotechnol. Adv.* **2013**, *31*, 1846−1859.
(6) Galbe, M.; Zacchi, G. *Biomass Bioenergy* **2012**, *46*, 70−78.
(7) Paroutis, P.; Touret, N.; Grinstein, S. *Physiology* **2004**, *19*, 207−215.
(8) Zhang, X.; Lin, Y.; Gillies, R. J. *J. Nucl. Med.* **2010**, *51*, 1167−1179.
(9) Charman, W. N.; Porter, C. J. H.; Mithani, S.; Dressman, J. B. *J. Pharm. Sci.* **1997**, *86*, 269−282.
(10) Boulane-Petermann, L. *Biofouling* **1996**, *10*, 275−300.
(11) Koch, M.; Bowes, G.; Ross, C.; Zhang, X.-H. *Glob. Change Biol.* **2013**, *19*, 103−132.
(12) Nishi, T.; Forgac, M. *Nat. Rev. Mol. Cell Biol.* **2002**, *3*, 94−103.
(13) Izumi, H.; Torigoe, T.; Ishiguchi, H.; Uramoto, H.; Yoshida, Y.; Tanabe, M.; Ise, T.; Murakami, T.; Yoshida, T.; Nomoto, M.; Kohno, K. *Cancer Treat. Rev.* **2003**, *29*, 541.
(14) Galster, H. *pH Measurement: Fundamentals, Methods, Applications, Instrumentation*; VCH: New York, 1991.
(15) Belyustin, A. A. *J. Solid State Electrochem.* **2011**, *15*, 47−65.
(16) Lin, J. *TrAC, Trends Anal. Chem.* **2000**, *19*, 541−552.
(17) Wencel, D.; Abel, T.; McDonagh, C. *Anal. Chem.* **2014**, *86*, 15−29.
(18) Janata, J. *Anal. Chem.* **1987**, *59*, 1351−1356.
(19) Sabnis, R. W. *Handbook of Acid-Base Indicators*; CRC: Boca Raton, FL, 2008, 398 pages.
(20) Nishimura, G.; Shiraishi, Y.; Hirai, T. *Chem. Commun.* **2005**, 5313−5315.
(21) Jiang, H.-L.; Feng, D.; Wang, K.; Gu, Z.-Y.; Wei, Z.; Chen, Y.-P.; Zhou, H. C. *J. Am. Chem. Soc.* **2013**, *135*, 13934−13938.
(22) Goicoechea, J.; Zamarreño, C. R.; Matías, I. R.; Arregui, F. J. *Sens. Actuators, B* **2008**, *132*, 305−311.
(23) Chen, S.; Liu, J.; Liu, Y.; Su, H.; Hong, Y.; Jim, C. K. W.; Kwok, R. T. K.; Zhao, N.; Qin, W.; Lam, J. W. Y.; Wong, K. S.; Tang, B. Z. *Chem. Sci.* **2012**, *3*, 1804−1809.
(24) Ma, X.; Wang, Y.; Zhao, T.; Li, Y.; Su, L.-C.; Wang, Z.; Huang, G.; Sumer, B. D.; Gao, J. *J. Am. Chem. Soc.* **2014**, *136*, 11085−11092.
(25) Cui, H.; Chen, Y.; Li, L.; Wu, Y.; Tang, Z.; Fu, H.; Tian, Z. *Microchim. Acta* **2014**, *181*, 1529−1539.
(26) Capel-Cuevas, S.; Cuéllar, M. P.; de Orbe-Payá, I.; Pegalajar, M. C.; Capitán-Vallvey, L. F. *Microchem. J.* **2011**, *97*, 225−233.
(27) Tsou, C.-J.; Chu, C.; Hung, Y.; Mou, C.-Y. *J. Mater. Chem. B* **2013**, *1*, 5557−5563.
(28) Zhang, X.; Li, Z.; Zhou, T.; Zhou, Q.; Zeng, Z.; Xu, X.; Hu, Y. *Talanta* **2016**, *150*, 184−189.

DOI: 10.1021/acs.analchem.7b01903
Anal. Chem. 2017, 89, 8437−8444

(29) Qian, Z.; Ma, J.; Shan, X.; Feng, H.; Shao, L.; Chen, J. *Chem. - Eur. J.* **2014**, *20*, 2254−2263.
(30) Vasylevska, A. S.; Karasyov, A. A.; Borisov, S. M.; Krause, C. *Anal. Bioanal. Chem.* **2007**, *387*, 2131−2141.
(31) Aigner, D.; Borisov, S. M.; Klimant, I. *Anal. Bioanal. Chem.* **2011**, *400*, 2475−2485.
(32) Strobl, M.; Rappitsch, T.; Borisov, S. M.; Mayr, T.; Klimant, I. *Analyst* **2015**, *140*, 7150−7153.
(33) Capel-Cuevas, S.; Cuéllar, M. P.; de Orbe-Payá, I.; Pegalajar, M. C.; Capitán-Vallvey, L. F. *Anal. Chim. Acta* **2010**, *681*, 71−81.
(34) Qi, J.; Liu, D.; Liu, X.; Guan, S.; Shi, F.; Chang, H.; He, H.; Yang, G. *Anal. Chem.* **2015**, *87*, 5897−5904.
(35) Zhang, M.; Sondergaard, R. V.; Kumar, E. K. P.; Henriksen, J. R.; Cui, D.; Hammershoj, P.; Clausen, M. H.; Andresen, T. L. *Analyst* **2015**, *140*, 7246−7253.
(36) Kolthoff, J. M. *Biochem. Z.* **1927**, *189*, 26−32.
(37) Lin, J.; Liu, D. *Anal. Chim. Acta* **2000**, *408*, 49−55.
(38) Gareis, T.; Huber, C.; Wolfbeis, O. S.; Daub, J. *Chem. Commun.* **1997**, 1717−1718.
(39) Hecht, M.; Kraus, W.; Rurack, K. *Analyst* **2013**, *138*, 325−332.
(40) Ma, X.; Cheng, J.; Liu, J.; Zhou, X.; Xiang, H. *New J. Chem.* **2015**, *39*, 492−500.
(41) Werner, T.; Wolfbeis, O. S. *Fresenius' J. Anal. Chem.* **1993**, *346*, 564−568.
(42) Liu, Z. H.; Luo, F. L.; Chen, T. L. *Anal. Chim. Acta* **2004**, *510*, 189−194.
(43) Opel, J.; Hecht, M.; Rurack, K.; Eiblmeier, J.; Kunz, W.; Cölfen, H.; Kellermeier, M. *Nanoscale* **2015**, *7*, 17434−17440.
(44) Foster, L. S.; Gruntfest, I. J. *J. Chem. Educ.* **1937**, *14*, 274−276.
(45) Loudet, A.; Burgess, K. *Chem. Rev.* **2007**, *107*, 4891−4932.
(46) Boens, N.; Leen, V.; Dehaen, W. *Chem. Soc. Rev.* **2012**, *41*, 1130−1172.
(47) Bell, J.; Climent, E.; Hecht, M.; Buurman, M.; Rurack, K. *ACS Sens.* **2016**, *1*, 334−338.
(48) Frisch, M. J.; et al. *Gaussian 03*, Revision D.01; Gaussian, Inc.: Wallingford CT, 2004.
(49) Gross, K. C.; Seybold, P. G.; Hadad, C. M. *Int. J. Quantum Chem.* **2002**, *90*, 445−458.
(50) Bartelmess, J.; Weare, W. W.; Latortue, N.; Duong, C.; Jones, D. S. *New J. Chem.* **2013**, *37*, 2663−2668.
(51) Kollmannsberger, M.; Rurack, K.; Resch-Genger, U.; Daub, J. *J. Phys. Chem. A* **1998**, *102*, 10211−10220.
(52) Baruah, M.; Qin, W.; Basaric, N.; De Borggraeve, W. M.; Boens, N. *J. Org. Chem.* **2005**, *70*, 4152−4157.
(53) Wang, J.; Hou, Y.; Li, C.; Zhang, B.; Wang, X. *Sens. Actuators, B* **2011**, *157*, 586−593.
(54) Urano, Y.; Asanuma, D.; Hama, Y.; Koyama, Y.; Barrett, T.; Kamiya, M.; Nagano, T.; Watanabe, T.; Hasegawa, A.; Choyke, P. L.; Kobayashi, H. *Nat. Med.* **2009**, *15*, 104−109.
(55) Descalzo, A. B.; Xu, H.-J.; Shen, Z.; Rurack, K. *Ann. N. Y. Acad. Sci.* **2008**, *1130*, 164−171.
(56) Bissell, R. A.; de Silva, A. P.; Gunaratne, H. Q. N.; Lynch, P. L. M.; Maguire, G. E. M.; Sandanayake, K. R. A. S. *Chem. Soc. Rev.* **1992**, *21*, 187−195.
(57) Trieflinger, C.; Röhr, H.; Rurack, K.; Daub, J. *Angew. Chem., Int. Ed.* **2005**, *44*, 6943−6947.
(58) Harriman, A.; Mallon, L. J.; Ulrich, G.; Ziessel, R. *ChemPhysChem* **2007**, *8*, 1207−1214.
(59) Rurack, K.; Kollmannsberger, M.; Resch-Genger, U.; Daub, J. *J. Am. Chem. Soc.* **2000**, *122*, 968−969.
(60) Lopez-Barbosa, N.; Gamarra, J. D.; Osma, J. F. *Anal. Bioanal. Chem.* **2016**, *408*, 2827−2837.
(61) Land-Zandstra, A. M.; Devilee, J. L. A.; Snik, F.; Buurmeijer, F.; van den Broek, J. M. *Public Underst. Sci.* **2016**, *25*, 45−60.
(62) Williams, A. J.; Pence, H. E. *J. Chem. Educ.* **2011**, *88*, 683−686.
(63) Hossain, M. A.; Canning, J.; Ast, S.; Rutledge, P. J.; Yen, T. L.; Jamalipour, A. *IEEE Sens. J.* **2015**, *15*, 5095−5102.
(64) Dutta, S.; Sarma, D.; Nath, P. *AIP Adv.* **2015**, *5*, 057151.
(65) Probe **1** shows only a 2-fold switching of the fluorescence due to an intense CT emission. On the other hand, choosing appropriate excitation and emission features yields enough resolution to be measured with the smartphone's CMOS and analyzed accordingly.
(66) Android Developers. *Android 5.1 APIs*, https://developer.android.com/about/versions/android-5.1.html (accessed May 10, 2017).
(67) Laha, J. K.; Dhanalekshmi, S.; Taniguchi, M.; Ambroise, A.; Lindsey, J. S. *Org. Process Res. Dev.* **2003**, *7*, 799−812.
(68) The present concept of using BODIPY probes and plastic accessories in combination with a smartphone is potentially suitable for future commercialization. As has been shown by Lindsey's group, synthetic upscaling to the 100 g-level is well possible for such compounds.[67] Moreover, today, the components of the device such as plastic holder, LED, wire, and filters (if alternative dye film filters are used) could also be mass-produced at considerably low prices. In addition, it might be possible to omit **6** and replace **8** by a mixture of **7** + **9** to reduce the costs while not compromising the performance of the system. Such attempts however would go beyond the scope of this article.

DOI: 10.1021/acs.analchem.7b01903
Anal. Chem. 2017, 89, 8437−8444